Advances in Physics Theories and Applications
ISSN 2224-719X (Paper) ISSN 2225-0638 (Online)
Vol.54, 2016

A Pragmatic Approach of Computational Methods for Simulation of Multiphase Flows

Arup Kumar Borah[1] Pramud Kumar Singh[2]
1 Department of Mathematics R G Baruah College, Gauhati University, Pin-781025 Assam, India
2 Department of Mathematics University of Allahabad, Uttar Pradesh Allahabad, U. P , Pin- 2266160, India

Abstract
In this paper we study the numerical simulation of multiphase flows which is a powerful tool for investigating and understanding the multiphase flows and to provide insight on the physics of free surface and interfacial flows such as bubble droplet dynamics, ocean wave motion, among others. The advanced in computational fluid dynamics and its extension to multi-fluid flows which is computational multifluid dynamics (CMFD) together with the increasing capacity of parallel computers have made possible to tackle such complex problems by using high performance numerical techniques such as direct numerical simulation (DNS). Direct numerical simulation is an important research area in modern CMFD. Moreover, DNS has a key role for improving the understanding of the multiphase phenomena and for using this technique for the simulation of flows in complex geometricians. The results from DNS is useful for developing better Eulerian-Eulerian and Eulerian-Lagrange methods. Furthermore, most of the DNS methods discussed in the literature have been restricted to Cartesian meshes and academic configurations. Thus the reasons are mainly due to the limited computational resources and because the standards algorithms are very complex to be efficient implemented on unstructured grids.
Keywords:Conservative level set method, Bubbly flow, Computational multi fluid dynamics, Navier Stoke's equation, Direct numerical simulation.

1. Introduction

We deal a numerical study of gravity-driven bubbly flow using a conservative level-set method (CLS). The shape and terminal velocity of a single bubble which rises in a quiescent liquid are calculated and contrasted against experimental and numerical results reported in the literature. Furthermore, different initial arrangements of bubble pairs are considered to study its hydrodynamic interactions. Finally, the gravity - driven bubbly flow is explored in the vertical duct with periodic boundary conditions. The results show the conservative level-set approach is able to accurately capture the deformation of interface on simulations of bubbly flows, and can remain numerically stable for a wide range of Morton and Reynolds numbers.

Bubbles play an important role in many natural and industrial processes. Steam generators in nuclear plants, rocket engines, unit operations in chemical engineering such as distillation. Absorption, extraction, heterogeneous catalysis and bioreactors are only a few among the multitude of applications that involve the motion of dispersed bubbles or drops in liquid. In industrial applications, such as bubble columns and the gas lift reactor (Mudde, 2005) , the flow usually involves swarms of bubbles created by a large numbers of nozzles or by a perforated plate with moderate to large bubble concentration, which offer large interfacial areas enhancing efficiency of heat and mass transfer. The current understanding of such flows and their predictive models are far from satisfactory because of the difficulty in describing hydrodynamics interactions of bubbles. Therefore, understanding fundamental behavior of bubble dynamics appear mandatory before a complete knowledge of bubble swarms can be achieved. Bubble interactions have significant consequences on bubble-size distribution, their breakup and coalescence behavior, and their understanding can help us to improve Eulerian-Lagrange or Euler-Euler modeling of bubbly flows. Recognition of this has motivated a large number of numerical and experimental researchers of bubble dynamics. Despite those efforts many challenging problems still remain as pointed out in recent reviews (Mudde, 2005 & Tryggvason, *et al.* 2013).

We studied (Bhaga and Weber,1981; Clift, e*t al.*1978; Hnat & Buckmaster 1976) and other provide a fairly detailed picture of the motion of bubbles rising through a quiescent viscous liquid for a wide range of Morton and Reynolds numbers. However, experimental studies of the interaction of two fluid particles are very limited. But, coalescence and bouncing of bubble pairs of *O* (1mm) in both pure water and aqueous surfactant solutions was studied (Duineveld, 1998) . There is a critical Weber number for the criteria of coalescence. The motion and wake of a pair of slightly deformed bubbles rising side by side in silicone oil and water (Sanada, *et al*. 2009) . We show that the patterns of the trajectories of rising bubbles are strongly dependent on the Reynolds number, furthermore, bubbles can collide each other above a critical Reynolds number. We studied (Takemure & Magnaudet, 2003) the transverse migration of both clean and fully contaminated spherical bubbles rising near a plane vertical wall in a quiescent viscous liquid of Reynolds number less than 100 using an optical technique. It is found that the lift force of clean spherical bubbles is directed away from the wall for $Re < 35$ and towards it for higher $Re > 35$. In the context of bubbly flow (Martinez-Mercado *et al*. 2007) in order to measure the velocities of both phases in a monodispersed bubbly flow in a vertical column, using water and water-glycerin mixtures, for a

range of Reynolds number from 10 − 500. We studied (Zenit *et al*.2001) concerning the averaged behavior of bubble suspensions of Large Reynolds number and moderately small Weber. Stewart (Stewart,1995) suggested how freely ellipsoidal bubbles approach each other, make contact, coalesce or break, or using swarms of 10-20 bubbles of low Morton number.

On the other hand, due to rapid development in computational power the Computational Multi-Fluid Dynamics (CMFD) has emerged as a powerful tool to study the bubble interaction mechanisms. Moreover, some numerical studies have been performed about bubble dynamics in recent years. Van Sint (Van Sint Annaland, *et al*.2005) demonstrated terminal Reynolds number and shapes of isolated gas bubbles rising in quiescent liquids by using volume-of-fluid method. Furthermore, (Hua *et al.* 2008), (Pivello *el al*. 2014) studied extensive on a single bubble rising in a quiescent liquid by using the front-tracking method. (Ohta *et al*.2010) suggested the effect of the density and viscosity ration on the motion of single drops rising in immiscible liquids using a coupled-level and volume-of-fluid method together with a sharp interface treatment of the interfacial jump conditions. On the other hand the same methodology is employed (Ohta & Sussman, 2012) to investigate the buoyancy-driven motion of a single skirted bubbles rising through a viscous liquid. (Baltussen *et al*.2014) studied different surface tension models for the volume-of-method in order to study single bubble rising in a quiescent liquid. (Ryskin and Leal, 1984) demonstrated a boundary fitted method on orthogonal coordinates to perform a numerical study of buoyancy-driven motion of single gas bubbles. (Chen *et al*. 2011) performed a two-dimensional simulation of the motion and coalescence of bubble pairs rising in a stationary liquid, using the moving particle semi-implicit method. (Smolianski *et al*. 2008) carried out two-dimensional simulations of the dynamics of single bubbles and small group of bubbles using the level-set-method. The Lattice-Boltzmann method was used by (Liu & Valocchi 2012; Gupt & Kumar, 2008; Cheng, *et al.*2010) to investigate the bubble motion and bubble coalescence in liquids. Yu *et al*. (2011) suggested a numerical study of bubble interaction using an adaptive Lattice-Boltzmann method. Chen *et al*.(1998); Hasan *et al*. (2011) applied the volume-of-fluid method to study the effects of liquid viscosity and surface tension of coalescence of two-coaxial bubbles. Pournader *et al*. (2013) suggested the effects of Reynolds number and viscosity of liquid film drainage mechanism formed during the interaction of two drops driven by buoyancy. A body fitted mesh has been applied Legendre & Magnaudet 2003) to investigate the interaction of two bubbles side by side. In this paper we have applied drag and transverse forces using some simple models based on a physical description of the interaction. Burner & Tryggvason (2002) *(*Burner & Tryggvason 2003; Burner & Tryggvason, 2003) characterized the rise velocity, microstructure and velocity fluctuations on swarms of spherical and ellipsoidal bubbles using the front tracking method.

Moreover, using the conservative level set method (Olsson & Kreiss 2005), (Olsson and Kreiss 2007) (Balcazar *et al.*, 2014) which is a promising technique for simulating two-phase flows with interfaces. The experimental and numerical studies cited above demonstrate that numerical investigations of bubble interactions and bubbly flows considering their coalescence are very limited in the scientific literature. In the present work we survey our results from three dimensional direct numerical simulations of buoyant bubbles by applying the conservative level- set (CLS) method. The objectives of this paper is to demonstrate the accuracy of the CLS method to predict bubble shapes and drag coefficient of single bubbles for various flow regimes and investigate hydrodynamic interactions mechanism for bubble pairs with different relative initial positions and also is to apply the CLS method to simulate the dynamic evolution of a suspension of many bubbles rising in a cylindrical wall confined domain, considering coalescence of bubbles when they collide.

2. Governing equations

For incompressible two-phase flows with uniform surface tension and no phase change, the Navier-Stokes equation, valid for the whole domain Ω and incorporating the jump conditions at the interface Γ are :

$$\frac{\partial}{\partial t}(\rho \mathbf{v}) + \nabla.(\rho \mathbf{v}\mathbf{v}) = -\nabla p + \nabla.\mu(\nabla \mathrm{v} + (\nabla \mathrm{v})^T) + (\rho - \rho_0)g + \sigma \kappa \mathrm{n} \sigma_\Gamma \quad (1)$$

$$\nabla.\,\mathrm{v} = 0 \quad (2)$$

Where v denotes the velocity vector, p being the pressure, g is the gravity acceleration, σ_Γ be the Dirac delta function concentrated at the interface, σ is the constant surface tension coefficient, κ is the curvature of the interface and **n** denotes the unite normal vector on the interface. Since ρ *and* μ are constant in |each fluid with a jump at the interface, and they can be represented as

$$\rho = \rho_1 H_1 + \rho_2(1 - H_1)\,;\ \mu = \mu_1 H_1 + \mu_2(1 - H_1) \quad (3)$$

Now the subscripts 1 and 2 denote fluid 1 and fluid 2, respectively, and H_1 is the Heaviside step function that is one at fluid 1 and zero elsewhere. Now for gravity driven bubbly flows in periodic domains, it is necessary to ensure that the resultant force in the direction of gravity is zero. Therefore, a force equal to the space-averaged density times the gravitational acceleration, ρ_0 g where $\rho_0 = \int_\Omega (H_1 \rho_1 + (1 - H_1)\rho_2)\, d\mathrm{V}$ is subtracted from the

right hand side of the Navier–Stokes equations. In the CLS method (Olsson & Kreiss 2005; Olsson and Kreiss 2007; Balcazar *et al.*, 2014) a regularized indicator function, ϕ is introduced for interface capturing:

$$\phi\,(\mathrm{x},t) = \frac{1}{2}\left(tanh\left(\frac{d(x,t)}{2\epsilon}\right)+1\right) \quad (4)$$

Where ε is a tunable parameter that sets the thickness of the profile. With the profile the interface Γ is defined by the location of the ϕ = 0.5 iso-surface, $\Gamma=\{x|\phi(x,t)=0.5\}$. Moreover, the conservative level set function ϕ is advected by a vector field **v** that is the given by the solution of the Navier-Stokes equation s. The interface transport equation can be written be conservative form provided the velocity field is solenoidal, $\nabla.\mathrm{v}=0$ as

$$\frac{\partial\phi}{\partial t}+\nabla.\phi\mathrm{v}=0 \quad (5)$$

Hence, an additional re-initialization equation is introduced to keep the profile and thickness of the interface constant,

$$\frac{\partial\phi}{\partial\tau}+\nabla.\phi(1-\phi)\mathbf{n}=\nabla.\epsilon\nabla\phi \quad (6)$$

This equation is advanced in pseudo-timeτ, and it consists of a compressive term $\phi(1-\phi)\mathbf{n}|_{\tau=0}$ which forces the level set function to be compressed onto the interface along the normal vector **n,** and for a diffusion term $\nabla.\epsilon\nabla\phi$ that ensure the profile remains of characteristic thickness ε . Geometric information on the interface, such as normal vector **n** or curvature κ, is obtained through,

$$n=\frac{\nabla\phi}{\|\nabla\phi\|} \quad (7)$$

$$\kappa(\phi)=-\nabla.\mathrm{n} \quad (8)$$

On the other hand we implement surface tension in a numerical scheme involve two issues: the curvature κ needs to be determined and the resulting pressure jump must be applied appropriately to the fluids. Now, the aforementioned problems can be conveniently addressed through the CSF method (Brackbill 1992). Thus, the singular term, $\sigma\kappa n\delta_\Gamma$ is converted to a volume force as follows,

$$\sigma\kappa n\delta_\Gamma=\sigma\kappa(\phi\,)\nabla\phi \quad (9)$$

Where $\kappa(\phi\,)$ is given by Eq. (10)

$$\kappa_i(\varphi_i\,)=-\nabla.n_i \quad (10)$$

Furthermore, in addition to the fluid properties are regularized by employing the level-set function,

$$\rho=\rho_1\phi+\rho_2(1-\phi)\,;\ \mu=\mu_1\,\phi+\mu_2(1-\phi) \quad (11)$$

3 Numerical method

Navier-Stokes equation has been discredited on a collocated unstructured grid arrangement by means of the finite-volume method (Balcazar *et al.*, 2014). Moreover, in order to avoid unphysical oscillations in the level-set function, TVD Superbee limiter is used to discretize the convective term of advection Eq. (5). We again central difference scheme is used to discretize both the convective and compressive terms of Eq.(1)and re-initialization of Eq. (6) respectively. A distance weighted linear interpolation is used to find the face values of physical properties and interface normal, while gradients are computed at cell centroids by using the least-square method. We solved the velocity-pressure coupling by means of a classical fractional step projection method. Now, momentum Eq. (1) is decomposed into two-steps

$$\frac{\rho\mathbf{v}^*-\rho\mathbf{v}^n}{\nabla t}=-\frac{3}{2}A_h\,(\rho\mathrm{v}^n\,)+\frac{1}{2}A_h((\rho\mathrm{v}^{n-1}\,)+D_h(\mathrm{v}^n\,)+\rho g+\sigma\kappa\nabla h(\phi) \quad (12)$$

$$\text{and } \mathrm{v}^{n+1}=\mathrm{v}^*-\frac{\Delta t}{\rho}\nabla_h(p^{n+1}) \quad (13)$$

where ∇_h denotes the gradient operator, $D_h\,(\mathrm{v})=\nabla_h.\mu(\nabla_h\mathrm{v}+\nabla_h^T\mathrm{v})$ represents the diffusion operator, and $A_h\,(\rho\mathrm{v})=\nabla_h.(\rho\mathbf{vv})$ denotes the advection operator. The resulting velocity v^* from Eq. (14)

$$\frac{\rho\mathbf{v}^*-\rho\mathbf{v}^n}{\nabla t}=-\frac{3}{2}A_h\,(\rho\mathrm{v}^n\,)+\frac{1}{2}A_h((\rho\mathrm{v}^{n-1}\,)+D_h(\mathrm{v}^n\,)+\rho g+\sigma_i^X\kappa_i\,\nabla_h(\varphi_i) \quad (14)$$

$$\nabla.\mathrm{v}=0 \quad (15)$$

Substituting Eq.(14) in Eq. (15) we obtain Poisson equation for pressure,

$$\nabla_h.\left(\frac{1}{\rho}\nabla_h(p^{n+1})\right)=\frac{1}{\Delta t}\nabla_h.(\mathbf{v}^*\,) \quad (16)$$

Now Eq. (16) after discretization leads to a linear system, which is solved by using a preconditioned conjugate gradient method. In order to avoid pressure-velocity decoupling when the pressure projection is made on collocated meshes (Rhie & Chow, 1983; Felten & Lund, 2006) a cell face velocity $\mathbf{v}_f$ can be defined so that $\nabla_h.\mathrm{v}=0$ in each control volume. The discretization form:

$$\mathrm{v}_f=\sum_{q\in\{P,F\}}\frac{1}{2}\left(\mathbf{v}_q^{n+1}+\frac{\Delta t}{\rho\,(\phi_q^n\,)}(\nabla h\,p^{n+1})q\right)-\frac{\Delta t}{\rho_f}(\nabla_h p^{n+1})_f \quad (17)$$

Where *P* and *F* be the adjacent cell nodes to the face *f*. In this study we consider for the temporal discretization, explicit Adams-Bashforth scheme is used for the momentum Eq.(12) , while for the corrector Eq. (13) an explicit

first order scheme has been applied. Advection Eq. (5) and Re-intitialization Eq. (6) and integrated in time with a 3-step third order accurate TVD Runge-Kutta method. Moreover, solving Eq. (6) to steady-state results in a smooth transition of ϕ at the interface that depends of the diffusion coefficient ϵ. In this paper, all numerical simulations were performed by setting $\epsilon = 0.5h$ where $h = (V_{cell})^{1/3}$ the characteristic size of the grid cell. Therefore, ϵ is chosen to be as small as possible in order to limit mass conservation errors, while maintaining reasonable resolution of the conservative level-set function to avoid numerical issues. In our simulations one-iteration per physical time-step of re-intialization Eq. (6) was sufficient to keep the profile of the level-set function. Furthermore, in the level-set method, coalescence happened automatically whenever two interfaces come within one grid cell of one another. Now, in the present simulations we allowed for possible coalescence and breakup of the bubbles.

Now, the time increment Δt , which is limited by the CFL conditions and the stability condition for the capillary force is given by,

$$\Delta t = 0.1\, min\left(\frac{h}{|v|}, \frac{\rho h^2}{\mu}, \left(\left(\frac{h}{|g|}\right)^{1/2}, h^{3/2}\left(\frac{\rho_1+\rho_2}{4\pi\sigma}\right)^{1/2}\right)\right) \qquad (18)$$

We have performed the global algorithm for solving the equations which are as follows

(i) calculating Δt from the Eq.(18), and solve level-set advection equation using Eq.(5).

(ii) It is solved re-initialization Eq.(6) for steady state, and hence calculating **v** and p by the fractional step method, Eq.(12), Eq.(16) and Eq. (13).

(iii) calculating $\mathbf{v}_f$ using Eq. (17), repeat step 2 to 7 until the desired time-level.

From the above algorithm the desired two-phase flow solver is computed in an in-house code Thermo Fluids (Lehmkuhl *et al.*, 2007), which is C++ (MPI) code designed for direct numerical simulation and large eddy simulation of turbulent flows (Trias & Lehmkuhl 2011; Rodriguez *et al.*,2011).

4. Results and discussion

Further, in order to test the ability of the CLS method for simulating different bubble regimes, now this section is devoted to investigate the dynamics of buoyancy bubbles. The bubble shape and its rise velocity, which is correlated to drag coefficient, is a complex function of the hydrodynamics, viscous and interfacial forces and experiments of (Bhaga & Weber 1981; Clift, 1978). We studied the relevant physical quantities in their experiments are $-\rho_g, \rho_l, \mu_g\ \mu_l, \sigma, d, g, U_T$ where $d = (6V/\pi)^{1/3}$ denotes the spherical volume equivalent diameter of the bubble, and U_T is the rise velocity. Now nondimensionalization results in the next parameters then we obtain,

$$M \equiv \frac{g\mu_l^4\,\Delta\rho}{\rho_l^2\sigma^3}, E_0 \equiv \frac{gd^2\Delta\rho}{\sigma}, R_e \equiv \frac{\rho_l U_T}{\mu_l} d, \eta_{\rho \equiv \frac{\rho_l}{\rho_g}}, \eta_\mu \equiv \frac{\mu_l}{\mu_g} \qquad (19)$$

where n_ρ, n_μ denotes the density and viscosity ratio respectively, M being the Morton number, $\Delta_\rho = \rho_l - \rho_g$, specifies the density difference between the fluid phases; E_0 is the EÖtvÖs number, and R_e is the Reynolds number. In this study, the Eötvös number is a characteristics of the bubble size and the Morton number is a parameter representing the viscosity of the liquid and we also introduce the non-dimensional time, $t^* = t\sqrt{\frac{g}{d}}$.

Moreover, the computational setup is schematically shown in Figure 1. In the initial state the spherical bubble is located on the symmetry axis of the cylinder. The numerical simulations are performed on a cylindrical domain of $(D_\Omega, H_\Omega) = (8d, 12d)$, now D_Ω, H_Ω denotes the cylinder diameter and cylinder height in the Figure 1, under periodic boundary conditions between the top and bottom boundaries, and Neumann boundary conditions at the side wall.

Figure 1. Computational system for single bubble simulations. (a) Sketch of initial condition and boundary conditions. (b) Mesh structure. (c) Mesh configuration.

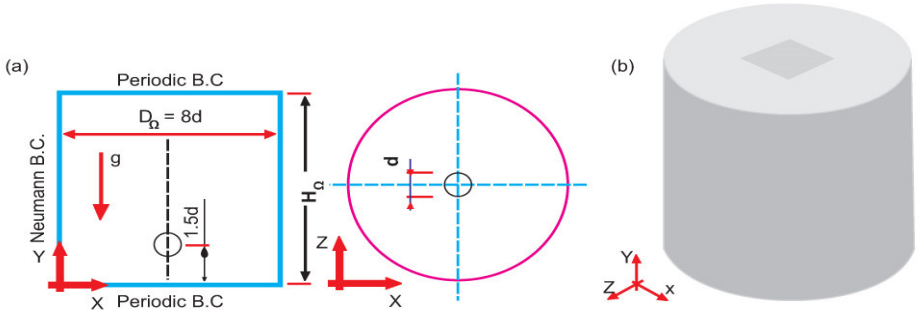

(c)

Mesh name	Mesh size	Cells per plane	Number of planes	$(D_{\Omega,}\ H_{\Omega,})$	h_{min}
M1	8.06E5	3360	240	(8d, 12d)	d/20
M2	1.41E6	4700	300	(8d, 12d)	d/25
M3	2.30E6	6405	360	(8d, 12d)	d/30
M4	1.87E6	5185	360	(6d, 12d)	d/30
M5	1.95E6	5529	360	(4d, 12d)	d/30
M6	3.07E6	6405	480	(8d, 16d)	d/30
M7	9.68E6	20160	480	(8d, 8d)	d/60

Mesh	Cell size	$(D_{\Omega,}\ H_{\Omega,})$	R_e	Relative error (ε_r)
M_1	h = d/20	(8d, 12d)	6.75	5.71%
M_2	h = d/25	(8d, 12d)	6.84	4.47%
M_3	h = d/30	(8d, 12d)	6.94	3.03%

Table 1: Influence of the grid size (h) on the Reynolds number, E_0 =116, M = 41.1, $\eta_\rho = 100$ and $\eta_\mu = 100$. Experimental reference $R_e = 7.16$ and mesh configuration and domain are shown in Figure 1.

Furthermore, with the intend of saving computational resources such as computational time and occupation of memory, our simulations are computed on a non-uniform hexahedral mesh, as shown in Figure 1(b). The mesh is generated by a constant step extrusion of a two-dimensional unstructured grid along the symmetry axis of the cylinder, being the step-size H_Ω / N_{planes}, where N_{planes} represents the number of planes in which the vertical axis is divided in Figure1.(b)-(c). But, the mesh is concentrated around the symmetry axis of the domain, where a uniform grid size h_{min} is fixed, to maximize resolution of the bubble. The mesh size grows exponentially to the border, when it reaches its maximum size $h_{max} \approx 10 h_{min}$ shown in Figure1 (b). Grid refinement and domain size studies are performed for the condition $E_0 = 116, M = 41.1, \eta_\rho = 100\ and\ \eta_\mu = 100$. Figure 2 (b) shows the variation in R_e as functions of dimensionless time t^* and Table 1 shows the value of the computed terminal Reynolds number and the relative error. Henceforth, the grid size is reduced; the relative difference of R_e between the successive meshes becomes small. Again from the Figure 1(b) and Table 2 display results obtained on different domain sizes, a decrease in cylinder diameter reduces the bubble rise velocity (Re), while the shape of the bubble remains almost unchanged (Harmathy 1960; Mukunda *et al.,* 2007; Van Sint Annaland, 2005; Hua *et .al.,*2008).

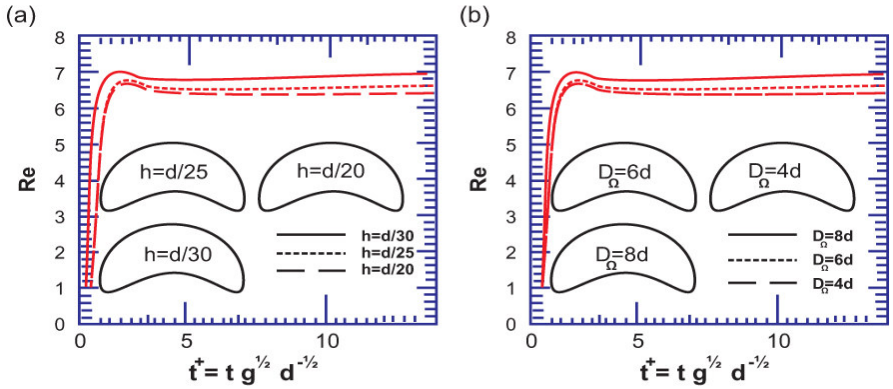

Figure 2: Grid and domain convergence for condition E_0= 116, M = 41.1, η_ρ=100, η_μ=100 .(a) Grid refinement convergence, D_Ω= 8d and H_Ω= 12d . (b) Domain size convergence h= d/30 and $H_\Omega = 8d$.

Mesh	Cell size	$(D_{\Omega,}\ H_{\Omega,})$	R_e	Relative error (ε_r)
M_4	h = d/30	(4d, 12d)	6.44	10.01%
M_5	h = d/30	(6d, 12d)	6.78	5.30%
M_6	h = d/30	(8d, 12d)	6.94	3.03%

Table 2: Influence of the grid size (h) on the Reynolds number, E_0 =116, M = 41.1, $\eta_\rho = 100$ and $\eta_\mu = 100$. Experimental reference $R_e = 7.16$ and mesh configuration and domain are shown in Figure 1.

Clearly it is observed that a domain size $(D_{\Omega,}\ H_\Omega) = (8d, 12d)$ and cell size $(h = d/30)$ are chosen at the standard

conditions for numerical tests is shown in Figure. 1.

Moreover, another important aspect to get accurate simulations is the mass conservation of the bubble phase as shown in Figure 3 and Table 3.

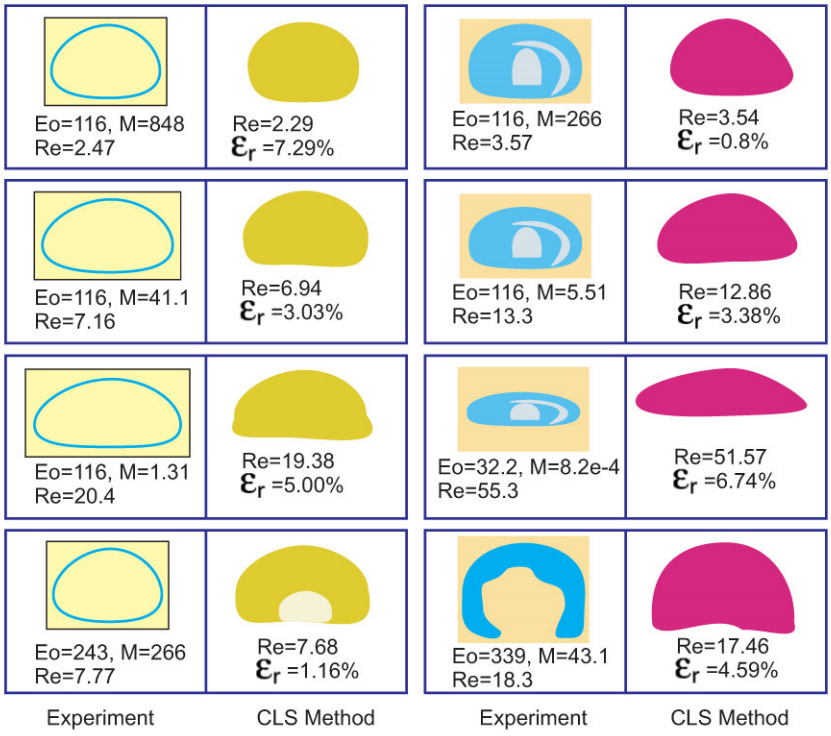

Figure 3: Comparison of terminal bubble shape and Reynolds number found (Bhaga & Weber, 1981) in experiments and the CLS method with mesh resolution h= d/30. The error in the Reynolds number is calculated by $\epsilon_r = \left|Re_{exp} - Re_{num}\right| Re_{exp}^{-1}$. All numerical experiments are carried out using $\eta_\rho = 100$ *and* $\eta_\mu = 100$.

E_0	M	Re			
		[4]--------[28]		Present	Mesh
116	848	2.47	2.317	2.29	M_3
116	266	3.57	3.621	3.54	M_3
116	41.1	7.16	7.0	6.94	M_3
116	5.51	13.3	13.17	12.86	M_3
116	131	20.4	19.88	19.38	M_3
32.3	8.2×10^{-4}	55.3	52.96	51.57	M_3
24.3	266	7.77	8.397	7.68	M_3
339	43.1	18.3	19.91	17.46	M_7

Table 3: A comparison of our computational results against experimental results of (Bhaga & Weber, 1981) and numerical results shown (Hua, *et al*. 2008) using the front-tracking method. Mesh configuration is shown in Figure 1.

The mass gain or loss may affect the shape of the interface and also the dynamics of the problem. Figure 4(a), shows the satisfaction of the requirement by an illustrative simulation for $E_0 = 116$, $M = 266$, $\eta_\rho = 100, \eta_\mu = 100$ and $h = d/30$.

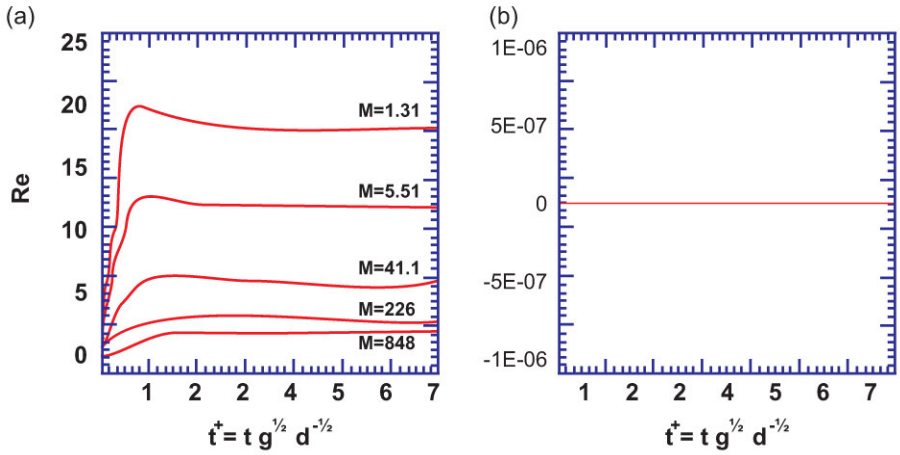

Figure 4: (a) Influence of Morton number (M) on terminal Reynolds number (Re). Re is plotted against the non-dimensional term (t^*), $h = d/30$, $E_0 = 116$, $\eta_\rho = 100$ and $\eta_\mu = 100$, (b) mass conversation of bubble phase , $E_0 = 116$, $M = 266$,

$\Delta m = \frac{m(t)-m(0)}{m(0)}$ where $m(t) = \int_\Omega \phi(x,t)\, dV$.

Furthermore, the bubble rising in the liquid, the instantaneous mass is calculated and compared with the initial mass, and hence the mass error is calculated by the expression such that $\Delta m = \left(m(t) - m(0)/m(0)\right)$ where$m(t) = \int \phi dV$. Now, from the Figure 4(b), the instantaneous mass of the bubble is conserved fairly well. This is one of the most interesting advantages of the CLS method.

We observe that the accuracy of the CLS method is investigated by comparison of the drag coefficient with experimental correlations and theoretical predictions. Hence, the drag coefficient C_D can be obtained from a simulation where the bubbles released in an initially quiescent liquid. Thus, from a steady state balance in the vertical direction C_D can be computed from the terminal rise velocity U_T,

$C_D = \frac{4(\rho_l - \rho_g)\|g\|d}{3\rho_l\ U_T^2}$

hence the relation in between C_D and R_e for fluids with Morton number $M > 4 >\times 10^{-3}$;

$C_D = ((2.67)^{0.9})\ ((\frac{16}{R_e})^{0.9})^{1/0.9}$ $\qquad M > 4 >\times 10^{-3}$ (19)

In these studies the numerical results are compared against the theoretical predictions of (Joseph, 2003). The drag coefficient is given

$$C_D = 0.445\ \left(6 + \frac{32}{R_e}\right) \quad (20)$$

Moreover, (Hadmard 1997; Rybczynski, 1998) we generalize the Stokes results for the viscous drag force on a solid sphere, to fluid particles of arbitrary and finite internal viscosity . After integration of pressure and shear stress on the fluid particle surface, they infer the drag coefficient at very low Re

$$C_D = \frac{8}{R_e}\left(\frac{2+3\eta_\mu^{-1}}{1+\eta_\mu^{-1}}\right) \quad R_e << 1 \quad (21)$$

In addition, a set of numerical simulations are carried out to calculate C_D from Eq.(18). From Figure 5(b) indicates the terminal Reynolds number as a function of dimensionless time, with $E_0 = 10, 10^{-3} \le M \le 10^2$, $\eta_\rho = 100$ and $\eta_\mu = 100$; whereas in Figure 5(a) shows the drag coefficient as a function of the Reynolds number- as M decreases , the bubble deformation increases and the spherical bubble approximations in Eq.(21) is valid for only high M, as one would indeed expect; moreover , numerical predictions of C_D are in a good agreement with Eq. (19) and Eq.(20). Now, the flow number (F) and the velocity number (V) as:

$$F = g\ \left(\frac{d^8\rho_l^5}{\sigma\mu_l^4}\right)^{1/3} \quad (22)$$

$$V = U_t\ \left(\frac{d^2\rho_l^2}{\sigma\mu_l}\right)^{1/3} \quad (23)$$

Which have been evaluated from the numerical results in Figure (5) and Table 3 for $E_0 = 10$ and $E_0 = 16$ respectively. Furthermore, the results are compared to the following correlations (Rodrigue, 2001):

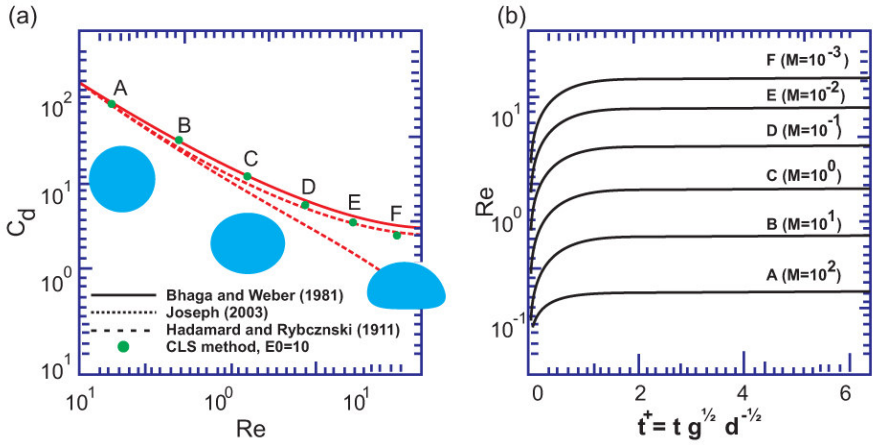

Figure 5: (a) Comparison of numerical prediction of drag coefficient C_D as a function of Reynolds number Re against Eq. (19) and Eq. (21); (b) Instantaneous Reynolds number as a function o dimensionless time t^*. Physical conditions are given by E_0 =10, $\eta_\rho = 100, \eta_\mu = 100,\ 10^{-3} \le M \le 10^3$ (low viscosity values).

$$V = \frac{F}{12\left(1+0.049F^{3/4}\right)} \qquad (24)$$

From the Figure 6 it is observed that numerical predictions are good agreement with the correlations given by the Eq.(23) and Eq.(24)

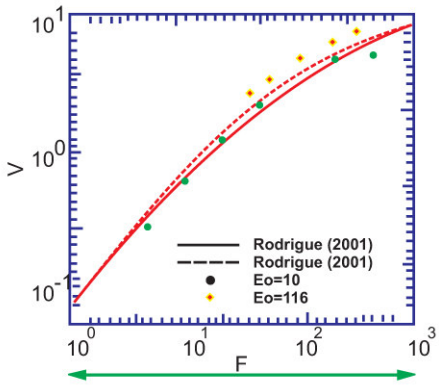

Figure 6: Velocity number (V) as a function of low number (F). Correlations are suggested (Rodrigue 2001).

$$V = \frac{F}{12(1+0.0185F)^{3/4}} \qquad (25)$$

Moreover, to further investigate the effect of density ratio on the terminal velocity U_t and bubble shape, we simulate a bubble rising under buoyancy for E_0 =39.4, M= 0.065, η_μ= 6.37×10^3 and η_ρ= {10,100,714}. In the present studies physical properties are chosen so that experimental results (Hnat & Buckmaster 1976) are equivalent to dimensionless parameters used in these studies.

Conclusions and Future works:

The achievements claimed by this paper are:

[i] a conservative level- set method has been used to study the dynamics of single and multiphase bubbles on a one-directional periodic domain.

[ii] the numerical method offers a high degree of accuracy in prediction of terminal Reynolds numbers, drag coefficient and the bubble shape for a wide range of E_0 and M numbers.

[iii] the methodology used in this studies is also capable of predicting the hydrodynamics interaction of bubble pairs and bubbles swarms.

[iv] hence the numerical results showed that bubble shapes, Reynolds numbers and wake patterns predicted by the CLS method agree well with experimental and numerical findings reported in the literature.

[v] in addition, numerical results of bubble pair interactions are in good agreement in agreement with numerical results published by using other methodologies.

[vi] now for the conditions selected in this paper (s=1.5d, $0^0 \ll \theta \ll 90^0$) both repulsive and attractive interactions are observed for spherical and ellipsoidal bubbles- which are a function of the Reynolds number and initial concentration angle.

[vii] the performed simulation with multiple bubbles demonstrates that CLS method can be employed to deliver useful information on the dynamics of bubbly flow.

[viii] to the best of the author's knowledge, the abovementioned 3 dimensional simulations of single and multiphase bubbles applying the CLS method are presented for the first time.

References

[1] MUDDE R. Gravity-Driven bubbly flows, *Annual Review of Fluid Mechanics* ., 37 (2005) 393–423.

[2] TRYGGVASON G., DABIRI S., ABOUHASANZADEH B. and JAICAI I., Multiscale consideration of direct numerical simulations of multiphase flows, *Physics of Fluids*., 25 (2013) 031302.

[3] BHAGA D. and WEBER M. E., *Journal of Fluid Mechanics*., 105 (1981) 61–85.

[4] CLIFT R., GRACEJ. R. and WEBER, M. E., Bubbles *Drops and Particles.* Academic Press, New York, (1978).

[5] HNAT J.G. and BUCKMASTER J. D., Spherical cap bubbles and skirt formation, *Physics of Fluids*., 19 (1976) 182–194.

[6] DUINEVELD P. C., Bouncing and coalescence and bubble pairs rising at high Reynolds number in pure water or aqueous surfactant solutions, *Appl. Sci Res.,* 58 (1998) 409–439.

[7] SANADA T., SATO A., SHIROTA M. and WATANABE M., Motion and coalescence of a pair of bubbles rising side by side, *Chemical Engineering Science.*, 64 (2009) 2659–2671.

[8] TAKEMURE F. and MAGNAUDET J., The transverse force on clean and contaminated bubbles rising near a vertical wall at moderate Reynolds number, *Journal Fluid Mechanics*., 495 (2003) 235–253.

[9] MARTINEZ-MERCADO J., PALACIOS-MORALES C.A. and ZENIT R., Measurement of pseudoturbulence intensity in monodispersed bubbly liquids for 10 <Re <500, *Physics of Fluids* ., 19 (2007) 103302.

[10] ZENIT R., KOCH, D. L. and SANGATI A. S., Measurement of average properties of a suspension of bubbles rising in a vertical channel, *Journal of Fluid Mechanics*., 429 (2001) 307–342.

[11] Stewart, C. W (1995), Bubble Interaction in Low-Viscosity Liquids, *International Journal of Multiphase Flow* 21, pp 1037–1046.

[12] VAN SINT ANNALAND, M., DEEN N.G. and KUIPERS, J.A.M., Numerical Simulation of gas bubbles behavior using a three-dimensional volume-of-fluid method, *Chemical Engineering Science*., 60 (2005) 2999–3011.

[13] HUA J., STENE J. and LIN P., Numerical Simulation of 3D bubbles rising in viscous liquids using front tracking method, *Journal of Computational Phys*., 227 (2008) 3358–3382.

[14] PIVELLO M. R., VILLAR M. M., SERFATY R., ROMA, A., M. SILVEIRA. And -NETO, A., A fully adaptive front tracking method for the simulation of two-phase flows, *International Journal of Multiphase Flow*., 58 (2014) 72 –82.

[15] OHTA M., YAMAGUCHI S., YOSHID A, and SUSSMAN M., The sensitivity of drop method motion due to the density and viscosity ratio, *Physics of Fluids.*, 22 (2010) 072102.

[16] OHTA M. and SUSSMAN M., The buoyancy-driven motion of a single skirted bubble or drop rising through a viscous liquid, *Physics of Fluids*., 24 (2012) 112101.

[17] BALTUSSEN M. W., KUIPERS J. A. M and DEEN N. G., A critical comparison of surface tensions models for the volume of fluid methods , *Chem. Eng. Sci.*, 109 (2014) 65–74.

[18] RYSKIN G. and LEAL L. G., Numerical solution of free boundary problems in fluid mechanics, Part 2 Buoyancy driven motion of a gas bubble through a quiescent liquid, *Journal of Fluid Mechanics*., 148 (1984) 19–35.

[19] CHEN R. H., TRAN W. X., SU G. H., QIU S. Z. and ISHIWTARI Y. OKA., Numerical investigation on a coalescence of bubble pairs, *Chem. Eng. Sci*., 66 (2011) 5055 –5063.

[20] SMOLIANSKI A., HARRIO H. and LUUKKA P., Numerical study of dynamics of single bubbles and bubble swarms, *Appl. Math. Model*., 32 (2008) 641–659.

[21] LIU H. and VALOCCHI A., Three-dimensional Lattice Boltzmann model for immiscible two-phase flow simulation, *Phys. Rev. Letters E*., 85 (2012) 046309.

[22] GUPTA A. and KUMAR R., Lattice Boltzmann Simulation to study multiple bubble dynamics, *International Journal of Heat and mass Transfer*., 51 (2008) 5192–5203.

[23] CHENG M., HUA J. and LOU J., Simulation of bubble-bubble interaction using a lattice Boltzmann method, *Computers and Fluids*., 39 (2010) 260–270.

[24] YU Z., YANG H. and FAN L., Numerical simulation of bubble interactions using adaptive lattice Boltzmann method, *Chem. Eng. Sci*., 66 (2011) 3441–3451.

[25] CHEN I., LI Y. and MANESH R., The coalescence of bubbles –A numerical study In: Third International Conference of Multiphase flow, (1998) ICMF 98, Lyon, France.

[26] HASAN N., ZAKARIA Z. B., Computational approach for a pair of bubble coalescence process, *International Journal of Heat and Fluid Flow*., 32 (2011) 755−761.
[27] POURNADER O. and MORTAZAVI S., Three dimensional interaction of two drops driven by buoyancy , *Computers and Fluids.*, 88 (2013) 543−556.
[28] LEGENDRE D. and MAGNAUDET J., Hydrodynamic interactions of two-spherical bubbles rising side by side in a viscous liquid, *Journal of Fluid Mechanics*., 497 (2003) 133−166.
[29] BURNER B. and TRYGGVASON G., Dynamics of homogeneous bubbly flows Part .1 Rise velocity and microstructures of bubbles, *Journal of Fluid Mech*. 466 (2002) 17−52.
[30] BURNER B. and TRYGGVASON G., Effect of bubble deformation on the properties of bubbly flows, *Journal of Fluid Mech.* 495 (2003) 77−118.
[31] ESMAEELI A. and TRYGGVASON G., A DNS study of the buoyant study of the rise of bubbles at O(100) Reynolds number, *Phys. of Fluids.* 17, (2005) 093303.
[32] OLSSON E. and KREISS G., A conservative level set method for two-phase flow, I, *Journal of Computational Physics .*,210 (2005) 225−246.
[33] OLSSON E. and KREISS G. A conservative level set method for two-phase flow, II, *J. Comput. Phys.,* 225 (2007) 785−807.
[34] BALCAZAR N., JOFRE L., LEHMKHUL O.,CASTRO, J., and Rigola J. (2014), A finite volume, level set-method for simulating two-phase flows on unstructured grids. *International Journal of Multiphase Flow.,*64 (2014) 55−72.
[35] BRACKBILL J.U., KOTHE D.B., and ZEMACH C. (1992), A continuum method for Modeling Surface Tension, *J. Comput. Phys.* 100 (1992) 335−354.
[36] RHIE C. M. and Chow W. L. Numerical study of the turbulent flow past an Airfoil with Trailing Edge Separation, (1983). *AIAAJ*, 21, 1525−1532.
[37] FELTEN F. N and LUND T. S., Kinetic Energy conservation issues associated with the collocated mesh scheme for incompressible flow, *J. Comput. Phys* 215 .(2006) 465−484.
[38] LEHMKUHL O., PEREZ-SEGARRA C. D., SORIA M and OLIVA A., A new parallel unstructured CFD code for the simulation of turbulent industrial problems on low cost PC cluster, *Proceeding of the parallel CFD* (2007) Conference, pp.1−8.
[39] TRIAS F.X. and LEHMKUHL O., A self-Adaptive strategy for the time integration of Navier-Stokes Equation. *Numerical Heat Transfer*, Part B 60, (2011) pp.116−134.
[40] RODRIGUEZ I., BORRELL R., LEHMKUHL O., PEREZ-SEGGRA, C. D and OLIVA A., Direct Numerical simulation of the flow over a sphere at Re = 3700, *J. Fluids Mech*. 679 (2011) 263â287.
[41] HARMATHY T. Z., (1960), Velocity of large drops and bubbles in media of infinite or restricted extend, *AI Ch E Journal* 6 (1960) 281−288.
[42] MUKUNDA K., QUAN, K., ECKMANN, S., AYYASWAMY,D.M P.S., Numerical study of wall effects on buoyancy gas- bubble rise in a liquid –filled finite cylinder , *Phys. Rev E*. 76 (2007), 036308-01â036308-15.
[43] JOSEPH D., Rise velocity of a spherical cap bubble, *J. Fluid Mech*. 488 (2003) 213−223.
[44] HADMARD J. S., (1997) Mo*vement permanent lent dâune sphere liquids et visqueuse dans liquid visquex,* C. R. Acad.Sci.1911, 152, 1735.
[45] RYBCZYNSKI W. (1998) *Uber die fortschreitende bewgung einer flssigen kugel in einem zhen medium*, Bull. Acad. Sci. Cracovi, Ser. 1911, A40.
[46] RODRIGUE D, (2001) Generalized correlations for bubble motion *AIChE Journal*, 47 (2001) 39−44.